 doi:10.20944/preprints201808.0366.v1

Article

Synthesis of Nanocrystalline-doped ZnO with Al^{3+} and Ni^{2+} by Sol-gel Method Coupled by Ultrasound Irradiation

M. J. Robles-Águila[1]*, J. A. Luna-López[1], Álvaro D. Hernández de la Luz[1], J. Martínez-Juárez[1], M. E. Rabanal[2]

[1] Benemérita Universidad Autónoma de Puebla, Instituto de Ciencias, Centro de Investigación en Dispositivos Semiconductores, Ciudad Universitaria, C. P. 72570, Puebla, Puebla, México jose.luna@correo.buap.mx, joalvada1@hotmail.com, javmartinez11@gmail.com

[2] Universidad Carlos III de Madrid e IAAB, Av. Universidad 30, 28911, Leganés, Madrid, España, eugenia@ing.uc3m.es

* Correspondence: josefina.robles@correo.buap.mx ; Tel.: +52-222-229-5500

Abstract: Zinc oxide is one of the most important semiconductor metal oxides and one of the most promising n-type materials, but its practical use is limited because of both its high thermal conductivity and its low electrical conductivity. Numerous studies have shown that doping with metals in ZnO structures leads to the modification of the band gap energy. In this work, Al-doped ZnO, Ni-doped ZnO, and undoped ZnO nanocrystalline powders were prepared by sol-gel method coupled with ultrasound irradiation. The doping concentration in ZnO was 1.0 at.% of Al and Ni. Influence of Al^{3+} and Ni^{2+} ions in the ZnO network are explored in this paper. X-ray Diffraction (XRD), Raman Spectroscopy, Nitrogen Adsorption (BET method), X-Ray Fluorescence (XRF) and Field Emission Scanning Electron Microscopy (FESEM) analyses demonstrated the incorporation of metal ions (aluminum and nickel) into the ZnO wurtzite structure. The crystallite size of the sample was decreased from 24.5 nm (ZnO) to 22.0 nm (ZnO-Al) and 21 nm (ZnO-Ni).

Keywords: Ultrasound irradiation; Doped; Zinc Oxide; Nanocrystalline; Powders

1. Introduction

Zinc oxide (ZnO) is a binary II-VI semiconductor compound with a hexagonal wurtzite structure and n-type electrical conductivity with a direct energy wide band of 3.37 eV and an exciton binding energy of 60 meV [1,2]. This semiconductor has high chemical, mechanical and thermal stabilities at room temperature, a low electrical constant, high electrochemical coupling index, wide range of radiation

 doi:10.20944/preprints201808.0366.v1

absorption and high photostability, all of which make it attractive for potential use in electronics, optoelectronics and laser technology [3].

ZnO is a transparent ceramic conducting oxide with interesting electrical and optical properties. Doped ZnO powders have several applications that include their use as a photocatalyst, ferromagnet, semiconductor, and piezoelectric and solar cells. This material has low resistivity and good optical gap energy at low temperature and is transparent in the visible region of the electromagnetic spectrum [4].

Many studies have been devoted to analyzing doped ZnO due to its several applications: solar cells, sensors, photoelectronic devices, diodes (LEDs), UV lasers, photocatalysts, field emitters, and spintronic and piezoelectric devices. Foreign metallic ions incorporated into the ZnO crystal lattice can modify the electronic properties of this semiconductor. On the other hand, some research have focused on doped ZnO films and powders prepared by several techniques such as sol-gel process [5], chemical bath deposition technique [6] solvothermal method [7], coprecipitation [8], hydrothermal synthesis [9], sputtering [10], spray pyrolysis method [11], microwave method [12], sonochemical method [13], mechanochemical method, microemulsion and combustion synthesis [3]. Incorporation of aluminum and nickel ions into ZnO can be achieved by different methods. Rajeh et al. studied the conductivity of doped ZnO using different metallic ions of group II and III (In^{3+}, Al^{3+}, Ga^{3+}, B^{3+}, Cu^{2+}, $Cd^{2+}$and Ni^{2+}) and suggested that conductivity is attributed to native defects or oxygen vacancies and zinc interstitial defects [14]. Transition metals doped with ZnO have been potential candidates to modify the electronic band structure and study their applications in semiconductor spintronic devices, spin polarized light emitting diodes, magnetic tunnel junctions, and photovoltaic cells and sensors [15,16]. Metallic ion doping increases the number of free electrons by replacing Zn^{2+} in the ZnO crystal lattice structure.

This paper aims at doping ZnO samples with Al^{+3} and Ni^{2+} by sol-gel method assisted by ultrasound irradiation, also referred to as sonochemistry. The physical phenomenon responsible for the sonochemical process is acoustic cavitation due to sonic radiation generated implosive collapse of bubbles increasing the temperatures (5000 to 25,000 K). For this reason, the ultrasound can break the bond of substances; make reaction times shorter in comparison with the conventional heating. The process starts with the creation of the nucleation center for their later growth until the obtained the nanocrystalline materials.

The samples were annealed at 450 °C to improve their physical properties and raise its crystallinity. We studied the effect of metallic ion substitution on the structural network and morphological properties of ZnO, as the effect of ultrasound irradiation in the process sol-gel for obtained nanomaterials. By doing a Rietveld

 doi:10.20944/preprints201808.0366.v1

refinement of the ZnO crystal structure, we found that incorporating Al^{3+} and Ni^{2+} into ZnO slightly changed cell parameters and network volume.

2. Materials and Methods

2.1 Synthesis of powders

Every chemical reagent used in the experiments was obtained from commercial sources as guaranteed-grade reagents and used without further purification. ZnO, ZnO-Al and ZnO-Ni were prepared using zinc acetate ($Zn(CH_3COO)_2$, Baker ACS), ethanol (C_2H_5OH, J. T. Baker, 99.6%), hydroxide ammonium (NH_4OH, Aldrich, 28%), nickel (II) chloride hydrate Puratronic ($NiCl_2 \bullet 6H_2O$, Alfa Aesar, 99.995%) and aluminum chloride ($AlCl_3$, Fermont, 99.4%). A zinc acetate solution in an ethanol and water mixture 50% (0.5 M) and NH_4OH was added dropwise with rapid magnetic stirring to achieve a pH 8.0 as some papers have reported that crystallinity and morphology are affected by pH value[17]. Next, this mixture was magnetically stirred for 1 h, and lastly, ultrasound irradiation over 30 min at intervals of 2 s was applied. In a similar procedure, ions of the corresponding salts were incorporated in 2 at. %. An ultrasonic processor from Sonics & Materials Inc. (Newton, CT, USA) was used and operated at 750 W and 20 kH. The resulting homogeneous solutions were filtered, and the products were washed with ionized water and ethanol several times to eliminate salts obtained from co-precipitation processes. The obtained gel was kept at room temperature to allow gelification over 72 h until a xerogel was attained. Then, the samples were ground in an agate mortar and heated in air in alumina crucibles in a muffle furnace at 450 ºC.

2.2 Characterization

XRD measurements were carried out using a Bruker D8 Discover with CuKα1 radiation ($\lambda_{\alpha 1}$ = 1.5406 Å). Data were collected over the 2θ range of 20-80 ° with a step size of 0.02. Phase composition of the samples was determined using the Powder Diffraction File PDF+4 from the ICDD (International Centre of Diffraction Data) [18]. Phase identification and Rietveld refinement of cell parameters were determined using the High Score Plus Software, including Powder Diffraction File PDF+4 from the ICDD. Input data for the Rietveld refinement (space group, cell parameters and atomic positions) were taken from T. M. Al-Saaid et al. [19]. A background was modeled by a polynomial approach, and a pseudo-Voigt function was used for the profile form. Then, a zero shift; a scale factor; unit cell parameters; U, W, V profile coefficients; and shape and asymmetric parameters were refined.

Al^{3+} and Ni^{2+} content in the doped powders were determined by wavelength-dispersive X-ray fluorescence (WDXRF) using a Bruker S8 Tiger spectrometer. The quantification of ions metals was realized with the Quant-Express method previous

 doi:10.20944/preprints201808.0366.v1

calibration of equipment. This measurement was carried out after preparation of 5 mm in diameter pellets with an applied pressure of 3.5 t cm^2.

Optical transmission spectra were recorded using a Varian Cary 400 Scan Spectrophotometer equipped with a Harrick DR accessory in a wavelength range of 200-800 nm. Teflon was used as a standard for the baseline. Raman spectra were measured with a spectrophotometer.

BET surface area was measured by nitrogen adsorption at 77 K using an Autosorb-1 after out-gassing at 398 K for 12 h. Morphological evaluation of the samples was carried out with a Field Emission Scanning Electron Microscopy measurement, FESEM (Hitachi SU-70) PL. Samples were excited by 375 nm using a NanoLog Spectrofluorometer Horiba NanoLog.

3. Results and Discussion

3.1 Structure from XRD Patterns and Raman Spectra

To investigate the influence of Al^{3+} and Ni^{2+} doping on the crystalline structure of ZnO, nanoparticles were measured by X-ray diffraction (XRD). Figure 1 shows the XRD powder pattern of ZnO, ZnO-Al and ZnO-Ni compared with PDF files of hexagonal (00-0361451) reported phases for ZnO. Diffraction peak characteristics correspond to the hexagonal wurtzite structure of pure ZnO in both doped samples with a preferential orientation along the (101) plane in every sample, as reported by Guruvammal et al.[20]. The insert in Figure 1 shows the main peaks (101), (002) and (101), where we can observe a shift towards lower angles and decreased intensity peaks due to an increased microstrain Ashokkumar [21] in doping ions Al^{3+} and Ni^{2+}. These results indicate that the presence of metal ions affects crystallite size [22].

Preprints (www.preprints.org) | NOT PEER-REVIEWED | Posted: 21 August 2018 doi:10.20944/preprints201808.0366.v1

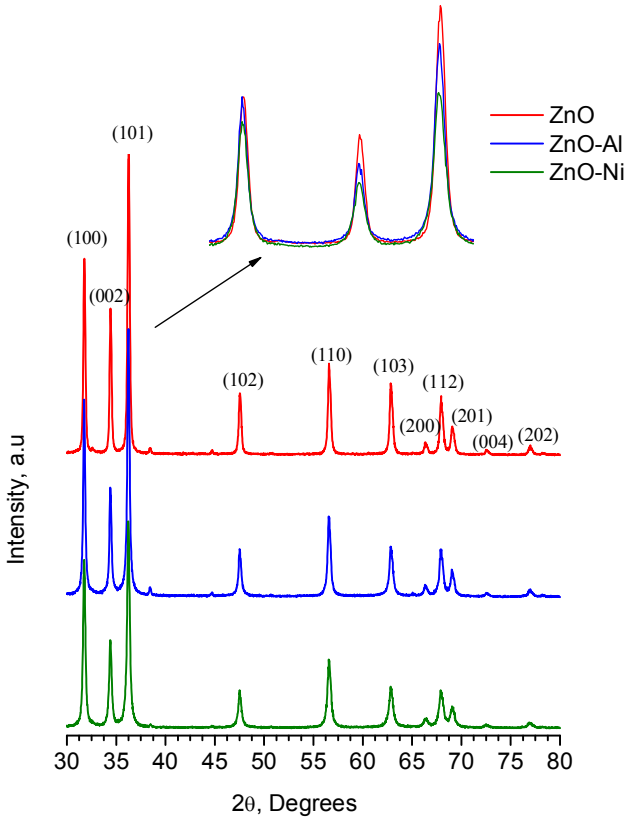

153

154 **Figure 1.** XRD powder patterns of ZnO and doped ZnO (Al^{3+} and Ni^{2+}). PDF file of hexagonal (00-
155 0361451). The inset shows the broadening and decrease of main peaks.

156

157 Katiyar et al. reported that the peak broadening is attributed to stress or particle
158 size variation due to the presence of other atoms in the network [23]. As there are
159 no diffraction peaks attributed to Al and Ni, related secondary phases are observed,
160 implying that the metal ions might substitute for the Zn atoms [24]. Theoretically,
161 since the ion radii have a coordination number of 4 (tetragonal site), Al^{3+} (0.053 nm)
162 and Ni^{2+} (0.069 nm) are smaller than those of Zn^{2+} (0.074 nm) [22,25]. These ions
163 should be able to substitute for Zn^{2+} ions in a ZnO matrix. Therefore, we propose
164 that Al^{3+} and Ni^{2+} are all well diffused in the ZnO lattice and doping has no
165 substantial effect on the hexagonal wurtzite structure.
166
167 The nominal values of crystallite size were determined with a module of PDF+4
168 2018 (Power Diffraction File) using every diffraction peak. Crystalline sizes of 22.0
169 nm for ZnO-Al and 21.0 nm for ZnO-Ni, which were small than that of ZnO (24.5
170 nm) obtained under the same conditions, were observed. P.K. Sharma et al. reported
171 the decreased in crystallite size due to of the incorporation of a foreign impurity
172 promoted the suppression of nucleation and subsequent growth rate due to ions
173 metals. By doing a Rietveld refinement of the crystal structure of samples, we found
174 that the Al^{3+} and Ni^{2+} incorporation into ZnO slightly changed the cell parameters.
175 Furthermore, Table 1 shows the refined cell parameters for doped samples, which

take the ZnO sample as a reference point. We considering only the hexagonal phase carried out this refinement.

Table 1. Table 1. Composition, structural and textural characteristics of the prepared samples.

Sample					Composition (by XRF)			Structural parameters		Textural parameters	
	a [Å]	*c* [Å]	V [Å^3]	R_{wp} [%]	% Zn	% O	% Ni, Al	Crystallite size t (nm)	Band gap E_g (eV)	S_{BET} ($m^2 g^{-1}$)	Average pore diameter (nm)
ZnO	3.252 (2)	5.209 (4)	47.72	8.45	75.0	25.0	0.00	21.0	3.60	22.0	68.0
ZnO/Al	3.252 (3)	5.211 (2)	47.35	8.27	71.0	29.2	0.80	22.0	3.44	23.0	33.0
ZnO/Ni	3.252 (1)	5.211 (5)	46.10	8.34	72.0	28.4	0.80	24.5	3.39	9.0	36.0

S_{BET}: specific surface, R_{wp}: weighted profile R-factor

The percentage of Al^{3+} and Ni^{2+} content incorporation into the ZnO structure was 1.0 at.%. We suggested that structure of ZnO only accepted approximately 50% of the nominal value in compare to the initial 2 at.%.

Raman spectra were recorded (Figure 2) under the same conditions for every sample. This technique is known to be susceptible to the local structure of ions, and it is now generally accepted that the positions and half-widths of the hexagonal bands are influenced by the preparation method, impurities and oxygen vacancies [26,27] Raman active modes of the wurtzite structure (space group P63mc) in the ZnO phase have six first-order vibrational modes, named A_1, E_1, $2E_2$ and $2B_1$, and are expected to appear near the point of their first Brillouin zone [28]. Raman spectra of ZnO, ZnO-Al and ZnO-Ni showed peaks at approximately 429 cm^{-1}, 490 cm^{-1}, 604 cm^{-1} and 707 cm^{-1}. An irrelevant broadening of the ZnO-Al and ZnO-Ni bands can be observed in comparison to the pure ZnO. The broadening of band E_1 may occur due to oxygen vacancies originated by the incorporation of Al^{3+} and Ni^{2+} ions into the hexagonal lattice. This result is agreed with the reported Luthra and Sayari [22,29].

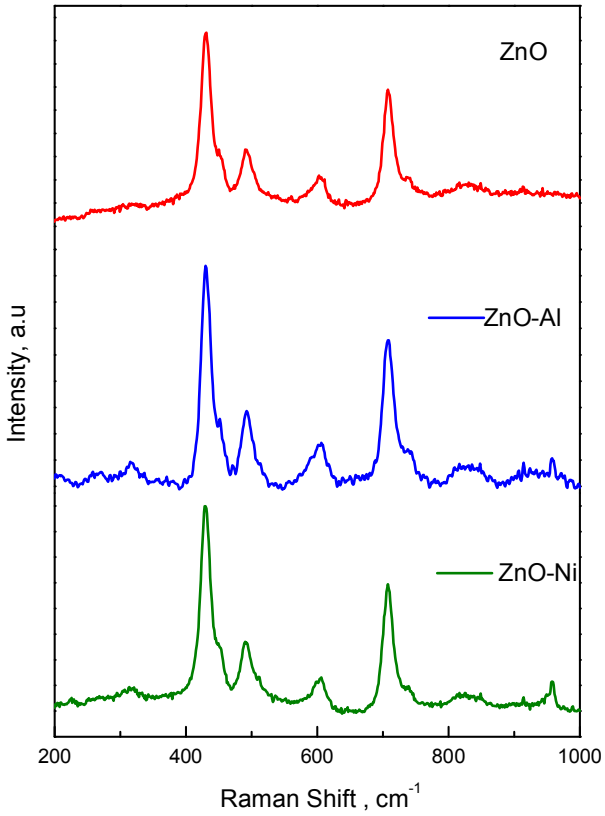

Figure. 2. Raman spectra of ZnO, ZnO-Al and ZnO-Ni samples obtained by sol-gel method assisted by ultrasound irradiation.

3.2 Optical properties

UV-Vis DRS spectra of the powders are shown in Figure 3. Spectra indicate the reflection percentage as a function of the band gap energy in the samples synthesized via ultrasound. The band gaps determined for ZnO and doped ZnO were 3.60 (ZnO), 3.44 (ZnO-Al) and 3.39 (ZnO-Ni) eV. This shift to the blue may be attributed to quantum confinement effects [16,30]. In doped ZnO samples, the absorption band gap was shifted to higher wavelengths due to interband transitions from the valence band A_{2g} to the T_{2g} level of Ni^{2+} ($3d^8$, $3A_{2g}$, $3T_{2g}$) by Ni^{2+}. Most authors observed that transition metal ions might additionally introduce d-d transitions into the UV-Vis spectra if the samples were present in a suitable oxidation state [1,27,31]. However, Al^{3+} increases free electrons by replacing Zn^{2+} in the ZnO network structure, hence generating conductivity in the semiconductor [24].

Preprints (www.preprints.org) | NOT PEER-REVIEWED | Posted: 21 August 2018 doi:10.20944/preprints201808.0366.v1

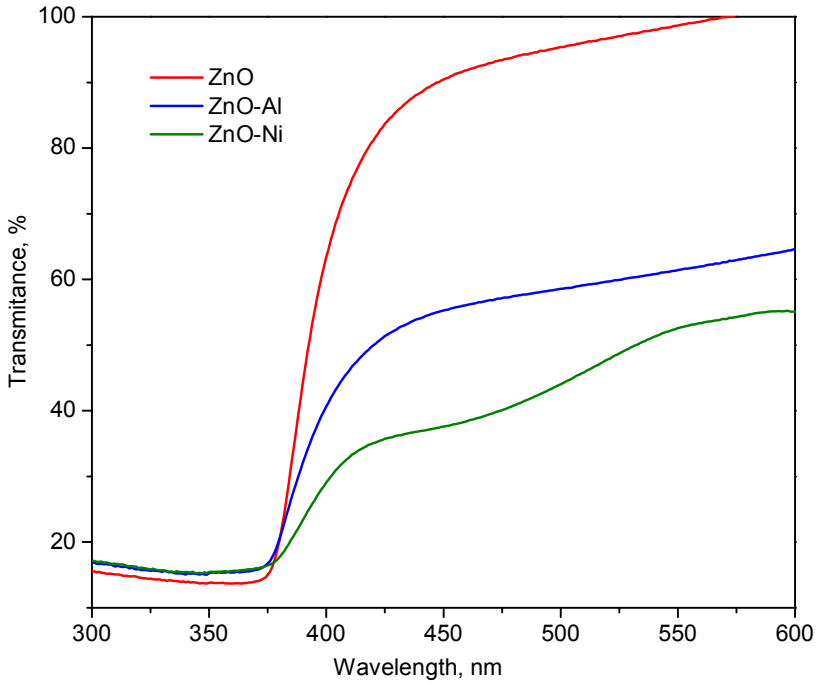

Figure. 3. Optical transmission spectra of ZnO and doped ZnO nanoparticles

In Figure 4, photoluminescence spectra of the undoped and doped ZnO samples show a broad and intense emission spreading from 425 to 650 nm with an emission at 590 nm, while doped ZnO samples show that a shift at 509 nm band is attributed to the presence of metal ions introduced by crystal defects such as oxygen vacancies because there are changes in the electronic band structure. This is agreed with Samadi et al, they reported that the oxygen vacancies enhanced the photo generation of electron-hole separation efficiency [1].

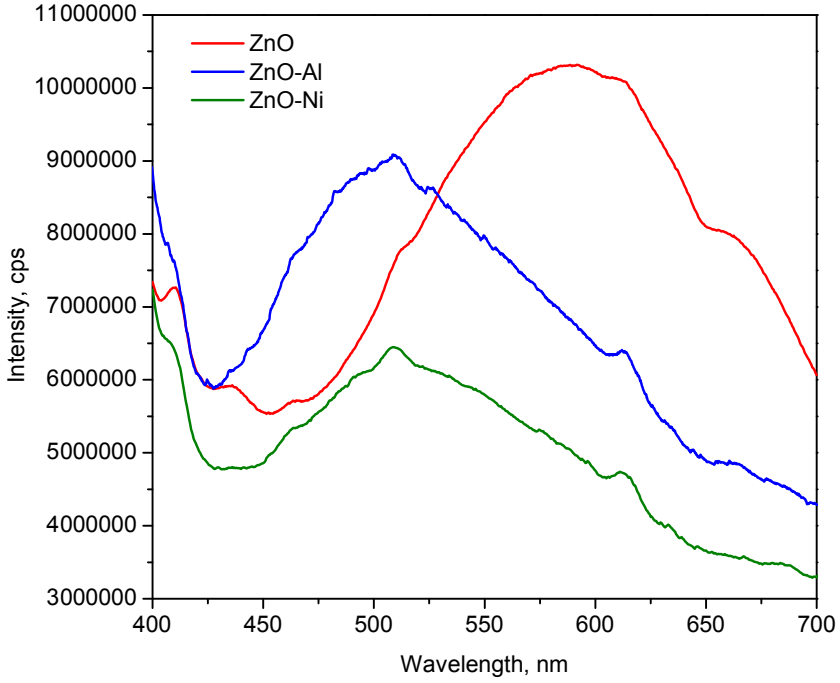

Figure. 4. Photoluminescence spectra of ZnO and doped ZnO (Al^{3+} and Ni^{2+}) nanoparticle samples.

 doi:10.20944/preprints201808.0366.v1

3.3 Surface morphological studies

Figure 5 shows the FESEM micrograph of ZnO, where we can see that the oxide semiconductor was formed by aggregates and sheets. In contrast, ZnO-Al and ZnO-Ni samples show agglomerate formations of sphere-shaped nanoparticles. We suggest that metal ions changed the surface shape of ZnO nanoparticles, the crystal size [1] and the mechanisms aggregation of nanoparticles. Therefore, SEM images implied that ion incorporation was one of the role factors affecting the surface morphology.

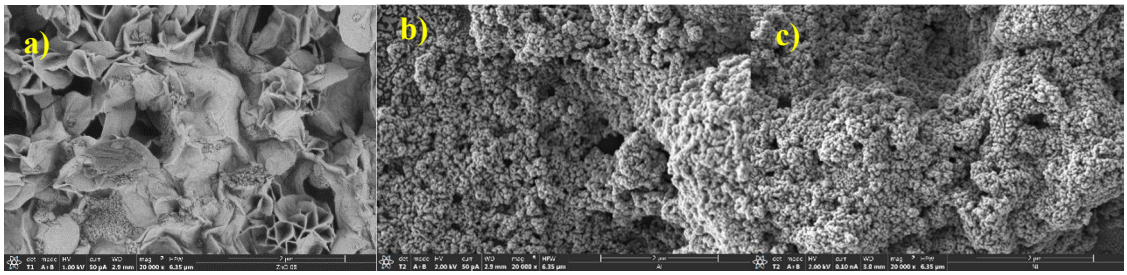

Figure. 5. FESEM images showing the morphology of nanocrystalline a) ZnO, b) ZnO-Al and c) ZnO-Ni.

3.4 Textural properties

The effect of doping aluminum and nickel on the textural characteristics of the powders prepared by sol-gel method assisted by ultrasound irradiation was investigated by measuring N_2 adsorption-desorption isotherms. Figure 6 shows the isotherm and pore size distribution of the doped samples, these isotherm exhibited a narrow hysteresis loop type H3 and a type II isotherm that may have been related to the agglomeration and slit-shaped spaces. In contrast with the pure ZnO, isotherm was IUPAC type II without a hysteresis loop. We suggest that the mesoporosity developed in the samples could have affected by the ultrasonic irradiation due to promote the incorporation of aluminum and nickel in to network of wurzite phase. The specific surface area (S_{BET}) and other textural parameters are compiled in Table 1. Results show a significant decrease in a pore average of doped samples according to the results obtained by SEM.

Preprints (www.preprints.org) | NOT PEER-REVIEWED | Posted: 21 August 2018 doi:10.20944/preprints201808.0366.v1

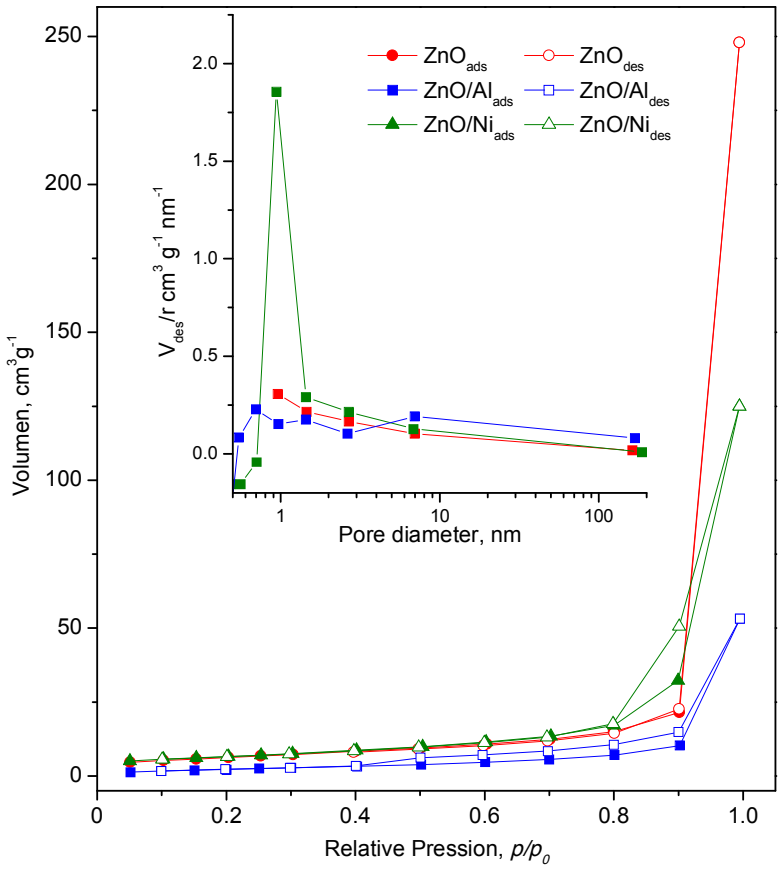

Figure. 6 Nitrogen adsorption-desorption isotherms and pore size distribution curves (inset) of ZnO, ZnO-Al, and ZnO-Ni, (filled circle, open circle). White symbols indicate adsorption, and black symbols indicate desorption

4. Conclusions

To sum up, we have researched the doped ZnO (Al^{3+} and Ni^{2+}) and undoped ZnO powders obtained by sol-gel method assisted by ultrasound irradiation. The sol-gel coupled ultrasound method is efficient to obtain nanomaterials in a short time reaction and to produce homogeneous nanometric particles with high crystallinity. Metal ion incorporation into the crystal structure of ZnO induces significant changes in morphological, optical and structural properties. The optical transmittance of the powders was greater than 80%. The optical direct band gap of films decreased from 3.60 to 3.44 and 3.39 eV, respectively, by doping at 1.0 at.% of Al^{3+} and Ni^{2+}. Finally, textural differences of nanocrystalline materials were observed in doped ZnO.

Author Contributions: M.J. Robles-Águila performed experiments and characterizations, analyzing the data and wrote the paper, M. E. Rabanal, J. Martínez Júarez and J.A Luna-López-Luna were made formal analysis and visualization, Álvaro D. Hernández de la Luz participated in the writing and final editing of the manuscript. All authors read and approved the paper.

Funding: The authors of this paper wish to thank Advanced Nanostructured Materials and Applications Network for its support via Secretaría de Educación Pública (SEP).

Acknowledgments: Author M. J. Robles-Águila wishes to thank the Powder Technology at Universidad Carlos III (UC3M) for its support and assistance in carrying out the experimental section. We are also grateful to Cristina Moral for her professional assistance (Laboratory SEM: UC3M) and Dr. Juan José Vilatela for his support in carrying out Raman Spectroscopy measurements at the IMDEA Materials Laboratory and Dr. A. Méndez-Blas for his assistance in the Photoluminiscence Spectroscopy measurements at the IFUAP Laboratory.

Conflicts of Interest: The authors declare no conflict of interested in this paper.

.

References

1. Samadi, M.; Zirak, M.; Naseri, A.; Khorashadizade, E.; Moshfegh, A. Z. Recent progress on doped ZnO nanostructures for visible-light photocatalysis. *Thin Solid Films* **2015**, *605*, 2–19, doi:10.1016/j.tsf.2015.12.064.

2. Morko *Zinc Oxide: Fundamentals, Materials and Device Technology*; 2009; ISBN 9783527408139.

3. Kolodziejczak-Radzimska, A.; Jesionowski, T. Zinc oxide-from synthesis to application: A review. *Materials (Basel).* 2014, *7*, 2833–2881.

4. Gahtar, A.; Benramache, S.; Benhaoua, B.; Chabane, F. Preparation of transparent conducting ZnO:Al films on glass substrates by ultrasonic spray technique. *J. Semicond.* **2013**, *34*, 073002, doi:10.1088/1674-4926/34/7/073002.

5. Mamat, M. H.; Khusaimi, Z.; Zahidi, M. M.; Mahmood, M. R. ZnO Nanorod Arrays Synthesised Using Ultrasonic-Assisted Sol-Gel and Immersion Methods for Ultraviolet Photoconductive Sensor Applications. *Nanorods* **2012**, 250, doi:10.5772/34828.

6. Son, N. T.; Noh, J.; Park, S. Role of ZnO thin film in the vertically aligned growth of ZnO nanorods by chemical bath deposition. *Appl. Surf. Sci.* **2016**, *379*, 440–445, doi:10.1016/j.apsusc.2016.04.107.

7. Lojkowski, W.; Gedanken, A.; Grzanka, E.; Opalinska, A.; Strachowski, T.; Pielaszek, R.; Tomaszewska-Grzeda, A.; Yatsunenko, S.; Godlewski, M.; Matysiak, H.; Kurzydłowski, K. J. Solvothermal synthesis of nanocrystalline zinc oxide doped with Mn 2+, Ni2+, Co2+ and Cr3+ ions. *J. Nanoparticle Res.* **2009**, *11*, 1991–2002, doi:10.1007/s11051-008-9559-9.

8. Shinde, K. P.; Pawar, R. C.; Sinha, B. B.; Kim, H. S.; Oh, S. S.; Chung, K. C. Optical and magnetic properties of Ni doped ZnO planetary ball milled nanopowder synthesized by co-precipitation. *Ceram. Int.* **2014**, *40*, 16799–16804, doi:10.1016/j.ceramint.2014.07.148.

9. Soomro, M. Y.; Hussain, I.; Bano, N.; Lu, J.; Hultman, L.; Nur, O.; Willander, M. Growth, structural and optical characterization of ZnO nanotubes on disposable-flexible paper substrates by low-temperature chemical method. *J. Nanotechnol.* **2012**, *2012*, doi:10.1155/2012/251863.

10. Siddheswaran, R.; Netrvalová, M.; Savková, J.; Novák, P.; Očenášek, J.; Šutta, P.; Kováč, J.; Jayavel, R. Reactive magnetron sputtering of Ni doped ZnO thin film: Investigation of optical, structural, mechanical and magnetic properties. *J. Alloys Compd.* **2015**, *636*, 85–92, doi:10.1016/j.jallcom.2015.02.142.

11. Than Htay, M.; Hashimoto, Y.; Momose, N.; Ito, K. Position-selective growth of ZnO nanowires by ultrasonic spray pyrolysis. *J. Cryst. Growth* **2009**, *311*, 4499–4504, doi:10.1016/j.jcrysgro.2009.08.008.

12. Li, D.; Wang, J.; Wu, X.; Feng, C.; Li, X. Ultraviolet-assisted synthesis of hourglass-like ZnO microstructure through an ultrasonic and microwave combined technology. *Ultrason. Sonochem.* **2013**, *20*, 133–136, doi:10.1016/j.ultsonch.2012.05.017.

13. Alammar, T.; Mudring, A.-V. Sonochemical Synthesis of 0D, 1D, and 2D Zinc Oxide Nanostructures in Ionic Liquids and Their Photocatalytic Activity. *ChemSusChem* **2011**, *4*, 1796–1804, doi:10.1002/cssc.201100263.

14. Rajeh, S.; Mhamdi, A.; Khirouni, K.; Amlouk, M.; Guermazi, S. Optics & Laser Technology Experiments on ZnO : Ni thin fi lms with under 1 % nickel content. *Opt. Laser Technol.* **2014**, *69*, 113–121, doi:10.1016/j.optlastec.2014.12.020.

15. Mani, G. K.; Rayappan, J. B. B. Selective detection of ammonia using spray pyrolysis deposited pure and nickel doped ZnO thin films. *Appl. Surf. Sci.* **2014**, *311*, 405–412, doi:10.1016/j.apsusc.2014.05.075.

16. Pal, B.; Sarkar, D.; Giri, P. K. Structural, optical, and magnetic properties of Ni doped ZnO nanoparticles: Correlation of magnetic moment with defect density. *Appl. Surf. Sci.* **2015**, *356*, 804–811, doi:10.1016/j.apsusc.2015.08.163.

17. Pal, U.; Serrano, J. G.; Santiago, P.; Xiong, G.; Ucer, K. B.; Williams, R. T. Synthesis and optical properties of ZnO nanostructures with different morphologies. *Opt. Mater. (Amst).* **2006**, *29*, 65–69, doi:10.1016/j.optmat.2006.03.015.

18. Kabekkodu, S. N.; Faber, J.; Fawcett, T. New Powder Diffraction File (PDF-4) in relational database format: Advantages and data-mining capabilities. *Acta Crystallogr. Sect. B Struct. Sci.* **2002**, *58*, 333–337, doi:10.1107/S0108768102002458.

19. Al-saadi, T. M.; Bakr, N. A.; Hameed, N. A. Study of nanocrystalline structure

and micro properties of ZnO powders by using Rietveld method. *Int. J. Eng. Tech. Res.* **2014**, *2*, 191–195.

20. Guruvammal, D.; Selvaraj, S.; Meenakshi Sundar, S. Effect of Ni-doping on the structural, optical and magnetic properties of ZnO nanoparticles by solvothermal method. *J. Alloys Compd.* **2016**, doi:10.1016/j.jallcom.2016.05.038.

21. Ashokkumar, M.; Muthukumaran, S. Effect of Ni doping on electrical, photoluminescence and magnetic behavior of Cu doped ZnO nanoparticles. *J. Lumin.* **2015**, *162*, 97–103, doi:10.1016/j.jlumin.2015.02.019.

22. Luthra, V.; Singh, A.; Pugh, D. C.; Parkin, I. P. Ethanol sensing characteristics of Zn0.99M0.01O (M = Al/Ni) nanopowders. *Phys. Status Solidi Appl. Mater. Sci.* **2016**, *213*, 203–209, doi:10.1002/pssa.201532447.

23. Huijuan Zhou Vivek Malik, Christoph Knies, Detlev M. Hofmann, Kanwal Preet Bhatti, S. Chaudhary, Peter J. Klar, Wolfram Heimbrodt, Claus Klingshirn, Heinz Kalt, L. C.; Zhou, H.; Chen, L.; {Huijuan Zhou Vivek Malik Detlev M. Hofmann, Kanwal Preet Bhatti, S. Chaudhary, Peter J. Klar, Wolfram Heimbrodt, Claus Klingshirn, Heinz Kalt,}, Limei Chen, C. K.; Pal, U.; Serrano, J. G.; Santiago, P.; Xiong, G.; Ucer, K. B.; Williams, R. T.; Pandey, R. K.; Mishra, S.; Tiwari, R.; Sharma, M. P.; Bajpai, P. K.; Xiong, G.; Pal, U.; Serrano, J. G.; Ucer, K. B.; Williams, R. T.; Us, C.; Dates, I.; Tracks, C.; Submission, P.; Publication, J.; Speakers, K.; Schedule, S.; Venue, C.; Committee, O.; Committee, T.; Us, C.; Yadav, H. K.; Sreenivas, K.; Gupta, V.; Katiyar, R. S.; Sayari, A.; El Mir, L. Structural studies and Raman spectroscopy of forbidden zone boundary phonons in Ni-doped ZnO ceramics. *Opt. Mater. (Amst).* **2015**, *3*, 381–386, doi:10.1063/1.2424538.

24. Sayari, A.; El Mir, L. Structural and optical characterization of Ni and Al co-doped ZnO nanopowders synthesized via the sol-gel process. *KONA Powder Part. J.* **2015**, *32*, 154–162, doi:10.14356/kona.2015003.

25. Shannon, R. D. Revised effective ionic radii and systematic studies of interatomic distances in halides and chalcogenides. *Acta Crystallogr. Sect. A* **1976**, *32*, 751–767, doi:10.1107/S0567739476001551.

26. Yadav, H. K.; Sreenivas, K.; Gupta, V.; Katiyar, R. S. Structural studies and Raman spectroscopy of forbidden zone boundary phonons in Ni-doped ZnO ceramics. *J. Raman Spectrosc.* **2009**, *40*, 381–386, doi:10.1002/jrs.2136.

27. Özgür, Ü.; Alivov, Y. I.; Liu, C.; Teke, A.; Reshchikov, M. A.; Doğan, S.; Avrutin, V.; Cho, S. J.; Morko, H. A comprehensive review of ZnO materials and devices. *J. Appl. Phys.* **2005**, *98*, 1–103, doi:10.1063/1.1992666.

28. Phuruangrat, A.; Thongtem, S.; Thongtem, T. Ultrasonic-assisted synthesis

and photocatalytic performance of ZnO nanoplates and microflowers. *Mater. Des.* **2016**, *107*, 250–256, doi:10.1016/j.matdes.2016.06.045.

29. Sayari, A.; El Mir, L. Structural and optical characterization of Ni and Al co-doped ZnO nanopowders synthesized via the sol-gel process. *KONA Powder Part. J.* **2015**, 154–162, doi:10.14356/kona.2015003.

30. Wang, N.; Yang, Y.; Yang, G. Great blue-shift of luminescence of ZnO nanoparticle array constructed from ZnO quantum dots. *Nanoscale Res. Lett.* **2011**, *6*, 338, doi:10.1186/1556-276X-6-338.

31. Pearton, S. J.; Norton, D. P.; Ivill, M. P.; Hebard, A. F.; Zavada, J. M.; Chen, W. M.; Buyanova, I. A. ZnO Doped With Transition Metal Ions. **2007**, *54*, 1040–1048.